Inorganic Chemistry

Article

pubs.acs.org/IC

New Three-Fold Interpenetrated Uranyl Organic Framework Constructed by Terephthalic Acid and Imidazole Derivative

Fei Chen,[†,‡] Cong-zhi Wang,[‡] Zi-jie Li,[‡] Jian-hui Lan,[‡] Yan-qin Ji,[†] and Zhi-fang Chai*[,‡,§]

[†]China CDC Key Laboratory of Radiological Pretection and Nuclear Emergency, National Institute for Radiological Protection, China CDC, Beijing 100088, People's Republic of China

[‡]Key Lab of Nuclear Radiation and Nuclear Energy Technology, Institute of High Energy Physics, Chinese Academy of Sciences, Beijing 100049, People's Republic of China

[§]School of Radiological&Interdisciplinary Sciences, Soochow University, Suzhou 215123, People's Republic of China

Supporting Information

ABSTRACT: A new 3-fold interpenetrated uranyl organic framework, UO_2(bdc)(dmpi), was hydrothermally synthesized using 1,4-benzenedicarboxylic acid (H_2bdc) and 1-(4-(1*H*-imidazol-1-yl)-2,5-dimethylphenyl)-1*H*-imidazole (dmpi). This framework, which was determined by synchrotron radiation X-ray, exhibited a new 3-fold interpenetrated (2,4)-connected topology with the Schläfli symbol of $(12^6)(12)_2$. Additionally, large incurvation happened to the bond angle of $[O{=}U{=}O]^{2+}$, which was always arranged in a rigorous line. Computational results based on density functional theory (DFT) indicated that the bent geometry of uranyl in UO_2(bdc)(dmpi) was mainly due to the higher charge populations in the valence 6d shells of uranium, rendered by the electronegative imidazoles.

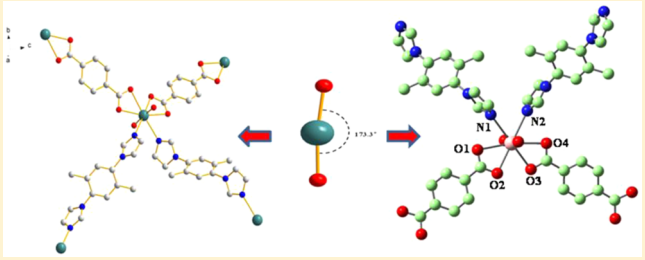

INTRODUCTION

In recent years, crystal engineering of metal organic frameworks (MOFs) has received increasing attention due to the potential applications in ion exchange,[1] separations,[2] nonlinear optics,[3] adsorption,[4,5] sensing,[6] catalysis,[7] and gas storage.[8,9] When transition-metal-based MOFs were well studied, people began to turn their research attention to lanthanides and actinides. Actinide organic frameworks have unique research significance besides the above-mentioned ones. By studying the coordination behavior of actinides with organic ligand, people can acquire basic principles to design extraction agents used in spent fuel reprocessing, and it is helpful to find out the novel precursors of nuclear fuels and the fabrication of waste forms.[10] As the most common species of uranium, uranyl always adopts rigorous linear arrangement and donor atoms of ligands typically bond to uranyl dication in equatorial planes, predominantly forming 1D or 2D structures.[11−15] It is a challenge to rationally design and synthesize 3D uranyl organic frameworks. Therefore, the number of uranyl complexes reported with extended 3D structures is far less than those of transition metals and lanthanides, not to mention interpenetrated ones.

Herein, we report the synthesis and structure of a new 3D uranyl organic framework, UO_2(bdc)(dmpi). It was constructed by 1,4-benzenedicarboxylic acid (H_2bdc) and 1-(4-(1*H*-imidazol-1-yl)-2,5-dimethylphenyl)-1*H*-imidazole (dmpi), which had a 3-fold interpenetrated structure. Similar work was reported only once before. In 2012, Zhong-Ming Sun and co-workers synthesized two 3-fold interpenetrated uranium organic frameworks for the first time.[16] Two semirigid ligands with flexible backbones, 4,4′-[[2-[(4-carboxyphenoxy)ethyl]-2-methylpropane-1,3-diyl]dioxy]dibenzoic acid and hexakis[4-(carboxyphenyl)oxamethyl]-3-oxapentane were incorporated in each structure. The second character of this framework is the remarkable incurvation of $[O{=}U^{VI}{=}O]^{2+}$. As we all know, the three atoms of UO_2^{2+} are always arranged in a rigorous line, exhibiting largely chemical inertness. However, a typical exception has never been reported. Also in 2012, Arnold and co-workers reported the structure of a binuclear uranium−oxo complex.[17] In the course of synthesis, UO_2^{2+} was reduced to UO_2^{+} first and two UO_2^{+} cations were delimited in a Schiff-base polypyrrolic macrocycle. The head-to-head oxygen atoms of two UO_2^{+} rearranged when they were close enough and formed a nonlinear $[O1{=}U1{=}O2]^{+}$ with an unusual bond angle of 173.4(2)°. Here, the reason for reducing the hexavalent uranyl to a pentavalent one was that the latter has larger chemical reactivity, and that was why oxygen could rearrange and form a nonlinear bond angle. The bond angle 173.3(5)° of UO_2^{2+} in UO_2(bdc)(dmpi) suggests the inertness of hexavalent uranyl could also be challenged to some extent. It is the first case of a 3-fold interpenetrated uranyl organic framework with a bending bond angle of uranyl. Furthermore, we try to explain the origin of bent uranyl units in UO_2(bdc)(dmpi) by density functional theory (DFT).

Received: January 4, 2015
Published: April 2, 2015

DOI: 10.1021/acs.inorgchem.5b00013
Inorg. Chem. 2015, 54, 3829−3834

EXPERIMENTAL SECTION

Synthesis. ***Caution!*** *Uranyl nitrate hexahydrate is a radioactive material. Suitable measures for precautions and protection should be taken, and all operations should follow the criterion while handling such substances.*

This uranium organic framework was prepared hydrothermally under autogenous pressure using 15 mL Teflon-lined stainless steel Parr autoclaves. The following reactants were used in synthesis: uranyl nitrate hexahydrate (Aladdin Reagent, 99.5%), H_2bdc (Sinopharm Chemical Reagent, 99%), dmpi (Acros, 98%), sodium hydroxide (Beijing Chemical Works, 99%), and ultrapure water (Resistivity 18.2 MΩ/cm). All chemical reactants were commercially available and used without any further purification.

UO_2(bdc)(dmpi). A mixture of $UO_2(NO_3)_4{\cdot}6H_2O$ (0.50 M, 0.1 mmol), H_2bdc (42.0 mg, 0.25 mmol), dmpi (48 mg, 0.2 mmol), and ultrapure water (4.0 mL) was placed in a 15 mL tightly closed Parr autoclave. The solution pH was adjusted to 6.5 with 1 M sodium hydroxide so as to make H_2bdc deprotonated. Then the autoclave was sealed and heated at 180 °C in an oven for 4 days. Subsequently, the autoclave was cooled naturally to ambient temperature. Yellow block crystals appeared accompanied by brown amorphous precipitates, which were then filtered off, washed with ultrapure water, and dried at room temperature for further characterization.

Crystallographic Studies. Diffraction data for UO_2(bdc)(dmpi) were collected at 100 K on the beamline station 3W1A of the Beijing Synchrotron Radiation Facility (BSRF). The parameters are listed below: wavelength, 0.72 Å; resolution, 0.70−50; distance, 60 mm; width, 3°; exposure time, 2.6 s. Diffraction data were processed using HKL-2000.[18] Structure determination was done by means of direct methods and refined employing full-matrix least-squares on SHELXL-97.[19] Selected crystallographic information is listed in Table 1. Atomic coordinates, bond distances, and additional structural information are provided in Tables S1 and S2, Supporting Information.

Table 1. Crystal Data and Structure Refinements for UO_2(bdc)(dmpi)

chemical formula	UO_2(bdc)(dmpi)
molecular weight	672.43
color	yellow
habit	block
space group	*C*2/*c*
a (Å)	10.674(2)
b (Å)	11.584(2)
c (Å)	18.116(4)
α (deg)	90.00
β (deg)	100.38(3)
γ (deg)	90.00
vol. (Å^3)	2203.3(7)
Z	4
T (K)	100(2)
λ (Å)	0.7500
max 2*θ* (deg)	25.67
ρ_{calcd} (g/cm^{-3})	1.221
$R(F)$ for $F_0^2 > 2\sigma(F_0^2)^a$	0.0411
GOOF	1.090

$^aR_1 = \sum(F_0 - F_c)/\sum F_0$. $R_2 = [\sum w(F_0^2 - F_c^2)^2/\sum w(F_0^2)^2]^{1/2}$.

Powder X-ray Diffraction and Fluorescence Spectra. The crystal phase of the synthesized material was examined by powder X-ray diffraction (XRD, Bruker D8 Advance) with a step size of 0.02° for Cu K*α* radiation (*λ* = 1.5406 Å). Fluorescence spectra of the powdered UO_2(bdc)(dmpi) were measured on a Hitachi F-4600 fluorescence spectrophotometer equipped with a xenon lamp and solid sample holder. The fluorescence spectrum of uranyl nitrate hexahydrate ($UO_2(NO_3)_2{\cdot}6H_2O$) is also presented for comparison.

Computational Methods. Density functional theory (DFT) calculations on the model species of UO_2(bdc)(dmpi) in the gas phase were carried out using the Gaussian 09 program package.[20] Geometries were optimized by the hybrid B3LYP[21,22] method without symmetry constraints. For uranium, the quasi-relativistic effective core potentials (RECP) including 60 core electrons were used to describe scalar relativistic effects, and the corresponding valence basis sets developed by the Stuttgart and Dresden groups[23−25] were adopted. The 6-311G(d, p) basis sets were used for carbon, nitrogen, oxygen, and hydrogen atoms. This level of theory has been found to yield accurate geometries for actinyl species.[26−28] The coordinates of terminal carbon and nitrogen atoms far away from the central uranium atom have been fixed during optimization to accurately simulate the crystal structure. Harmonic vibrational frequency calculations were carried out at the B3LYP/RECP/6-31G(d) level of theory to verify the minima character of the geometrical structures. In order to provide insight into the bonding nature, natural bond orbital (NBO) analysis, Mayer bond order (MBO), and natural population analysis (NPA)[29−33] were performed at the same level of theory.

RESULTS AND DISCUSSION

Structure Description. UO_2(bdc)(dmpi) crystallizes in the space group *C*2/*c* with cell parameters *a* = 10.674(2) Å, *b* = 11.584(2) Å, *c* =18.116(4) Å, and *β* = 100.38 (3)°. As shown in Figure 1 a, two rigid ligands (Scheme 1), H_2bdc and dmpi, are

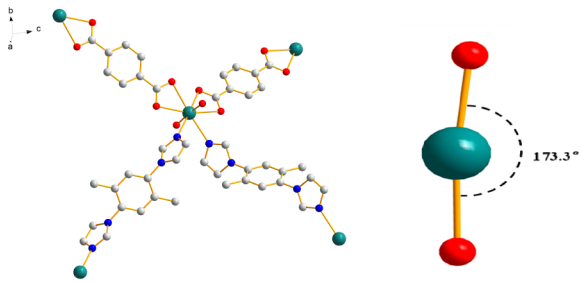

Figure 1. (a) Asymmetric unit of UO_2(bdc)(dmpi). (b) Bond angle of UO_2^{2+}. U atoms are represented in green, O in red, C in gray, and N in blue. All H atoms are omitted for clarity.

Scheme 1. Structures of Ligands

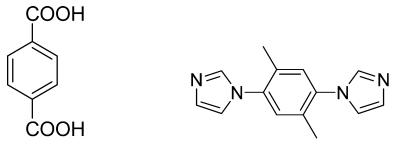

both incorporated into UO_2(bdc)(dmpi) and their multi-coordination sites contribute to formation of the 3D structure. Each uranyl adopts a 6-coordinate geometry in the equatorial planes, defined by four O atoms and two N atoms, which are assigned to two deprotonated H_2bdc and two dmpi molecules, respectively. Axially, the bond angle of O═U═O is 173.3(5)° (Figure 1 b), which is significantly deviated from normal. This implies the change of uranyl reactivity in the current coordination environment. The lengths of U═O are both 1.773(8) Å, while the lengths of U−O in the equatorial plane are 2.496(8) and 2.502(8) Å, and the U−N bond length is

DOI: 10.1021/acs.inorgchem.5b00013
Inorg. Chem. 2015, 54, 3829−3834

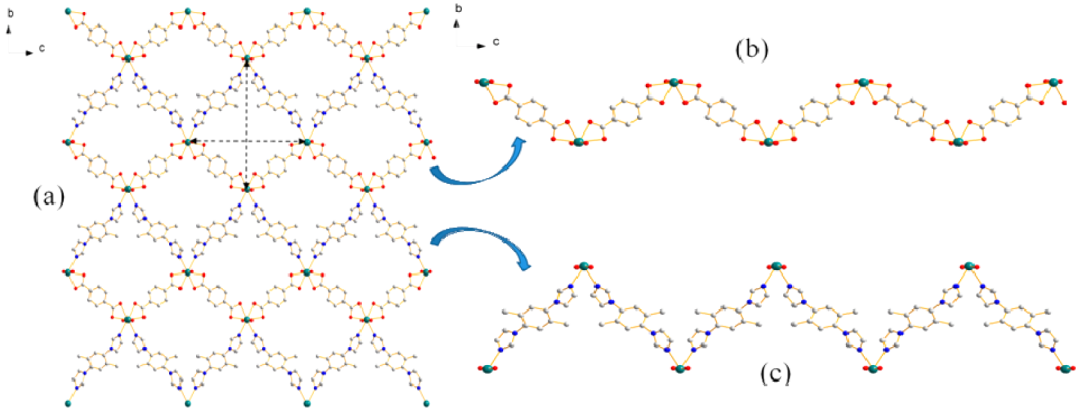

Figure 2. (a) Singlet network of $UO_2(bdc)(dmpi)$, viewing along the *a* axis. (b) One typical sheet abstracted from a. (c) Another fluctuating sheet abstracted from a.

2.550(9) Å. Other bond lengths and bond angles are listed in Tables S1 and S2, Supporting Information.

$UO_2(bdc)(dmpi)$ has a 3-fold interpenetrated framework. In order to clearly present the 3-fold interpenetrated structure, $UO_2(bdc)(dmpi)$ was split into three singlet molecules. Viewing along the *a* axis (Figure 2a), the singlet molecule of $UO_2(bdc)(dmpi)$ presents an infinite network in which four edges of the irregular quadrangle are constituted by two deprotonated H_2bdc and two dmpi molecules, generating the network with a size of 18.18 Å × 19.30 Å. In another perspective, this network can also be regarded as the combination of two types of fluctuating sheets. One type is made up of uranyl and bdc^{2-} (Figure 2b), and another is composed of uranyl and dmpi (Figure 2c). Viewing along the *c* axis (Figure 3), the singlet molecule of $UO_2(bdc)(dmpi)$ exhibits another infinite network, in which the channels seem like squashed hexagons with a size of 25.32 Å × 19.30 Å.

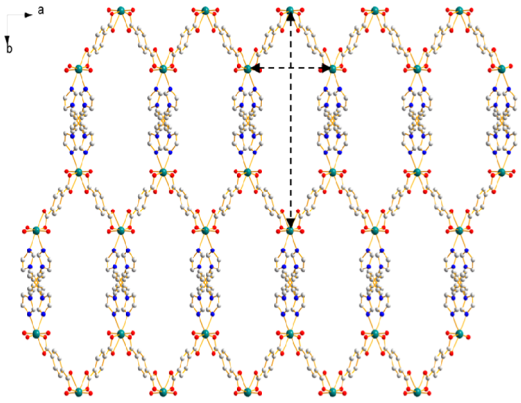

Figure 3. Packing diagram of the singlet molecule, viewing along the *c* axis.

It can be seen in Figures 2 and 3 that the singlet molecule of $UO_2(bdc)(dmpi)$ has a large void volume. Therefore, triple equivalent molecules can interpenetrate one another to keep the stability of the whole structure. To understand the complicated configuration, topological analyses were utilized in which the ligands were simplified to 2-connected nodes. After simplification, the structure of $UO_2(bdc)(dmpi)$ exhibits a 3-fold interpenetrated (2,4)-connected topology with the Schläfli symbol of $(12^6)(12)_2$. When viewing along the *a* axis, the network of a singlet molecule can be represented as shown in Figure 4a, and it represents the topology of Figure 2a as well. Three-fold interpenetrated topologies are shown in Figure 4b, in which triple equivalent interpenetrated molecules are depicted in red, yellow, and blue. In addition, Figure 4c illustrates the topology of triple equivalent interpenetrated molecules viewing along the *b* axis. Calculated in PLATON,[34] the void space of $UO_2(bdc)(dmpi)$ amounts to only 3.5%, which reveals the void volume has been filled with the interpenetrated molecules.

DISCUSSION

When this structure was refined, large incurvation was found accidentally in uranyl ions. After much deliberation, two different hypotheses were proposed on the reasons for incurvation. The first one is that the bending is caused by interpenetration. O═U═O in a singlet molecule was originally arranged linearly, and its protruding O atoms had certain steric hindrance. When the molecule was penetrated by another, the O atoms might give their way; thus, bending occurred to the uranyl ion. The second is assigned to the effect of the imidazole rings around the uranyl ions. It is well known that imidazole is an aromatic heterocyclic compound with large charge density. When U−N bonds formed, imidazole rings exhibited notable affinity to uranyl ions and induced the electron transformation in orbits of uranium. Thus, bending occurred in uranyl ions for the change of electron orbits. However, two proposed hypotheses need to be confirmed by more evidence.

Computational Study. For further insight into the incurvation and bonding nature of $UO_2(bdc)(dmpi)$, a model species of the uranyl organic framework has been studied using DFT. Figure 5 shows the optimized structure of the mode fragment. As can be seen, the geometry optimized at the B3LYP/6-311G(d, p)/RECP level of theory agrees well with the experimental structure determined by X-ray diffraction, which is an eight-coordinate structure with two bidentate bdc^{2-} ligands and two dmpi ligands in the equatorial plane of the uranyl ion. As listed in Table 2, the DFT-optimized bond distances for the model species are found to be in very good accord with the experimental data, and the discrepancy between the calculated and the experimental bond distances is less than 0.06 Å. In addition, the calculated O═U═O angle for $UO_2(bdc)(dmpi)$ is 170.6°, which compares well to the corresponding experimental value of 173.3(5)°.

The calculated Wiberg bond indices (WBIs) and Mayer bond orders (MBOs) of the U−O and U−N bonds are also

DOI: 10.1021/acs.inorgchem.5b00013
Inorg. Chem. 2015, 54, 3829−3834

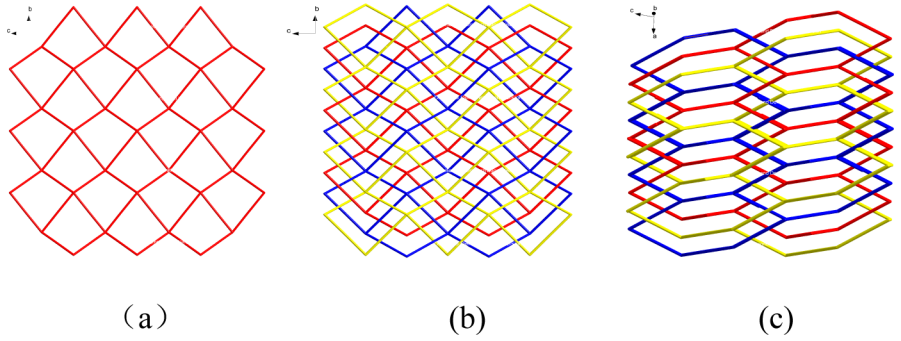

Figure 4. (a) Topology representation of the singlet network, viewing along the *a* axis. (b) Topology representation of a 3-fold interpenetrated network, viewing along the *a* axis. (c) Topology representation of a 3-fold interpenetrated network, viewing along the *b* axis.

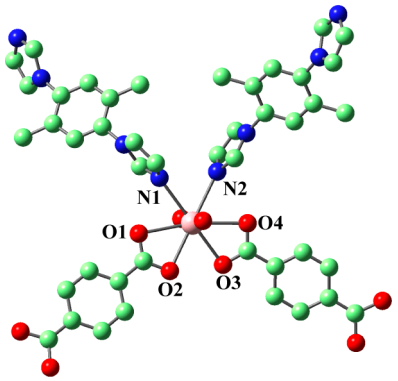

Figure 5. Optimized structure for the model species of UO_2(bdc)(dmpi). Red, green, blue, and pink spheres represent O, C, N, and U, respectively (hydrogen atoms were omitted for clarity).

Table 2. Comparison of Selected Calculated and Experimental Bond Lengths (Angstroms), and the WBIs and MBOs of the U−O and U−N Bonds for the Model Species of UO_2(bdc)(dmpi)

bond	expt	calcd	WBIs	MBOs
U═O(axial)	1.773(8)	1.792	2.167	2.102
U−O1	2.502(8)	2.513	0.468	0.431
U−O2	2.496(8)	2.436	0.525	0.448
U−O3	2.496(8)	2.436	0.525	0.448
U−O4	2.502(8)	2.513	0.468	0.431
U−N1	2.550(9)	2.619	0.382	0.179
U−N2	2.550(9)	2.619	0.382	0.179

summarized in Table 2. In general, the WBIs and MBOs of these bonds are between 0.1 and 0.6, indicating the small covalent character of the bonding. Compared to the U−N bonds, the U−O bonds show slightly higher bond orders. Besides, the electron localization function (ELF)[35,36] (Figure S3, Supporting Information) results also suggest that the U−O bonds have a higher degree of covalent character than the U−N bonds. According to natural population analysis, the calculated natural charge on uranium is 1.389, which is much smaller than that of the free uranyl cations (2.736). This suggests significant charge donation from the ligands to uranium. Moreover, net charges of the oxygen atoms in the bdc ligands and the nitrogen atoms in the dmpi ligands are about −0.6 and −0.5, respectively, which indicates that the bidentate bdc ligands have stronger coordination ability to the uranyl cations than the monodentate dmpi ligands.

As mentioned above, UO_2(bdc)(dmpi) has an unusual structure because it possesses a rare bent uranyl with a O═U═O bond angle of 173.3°, which is consistent with the calculated O═U═O bond angle of 170.6° for UO_2(bdc)(dmpi). This result can help to exclude the first hypothesis. According to this data, the incurvation remains even in the optimized mode fragment, which is only a representative part of the singlet molecule. Therefore, it can be concluded that the bending has no direct relationship with the structure interpenetration.

Previous theoretical studies[37−40] on linear and bent actinyls indicate that the 6d and 5f orbitals of actinides are mainly involved in the metal−ligand bonding. Additionally, the actinide 5f orbitals prefer linear geometries, while the 6d orbitals are more effective for bent structures. To explore the bent geometry of the uranyl unit in UO_2(bdc)(dmpi), Mulliken orbital population analysis has been performed at the B3LYP/6-311G(d, p)/RECP level of theory. For comparison, we also calculated Mulliken orbital populations for the free uranyl cation at the same level of theory, which exhibits linear geometry with a O═U═O angle of 180.0°. The calculated results of the valence s, p, d, and f shells for the uranium in UO_2(bdc)(dmpi) and the free uranyl cation are shown in Table 3.

Table 3. Calculated Mulliken Orbital Populations (s, p, d, and f) for Uranium of the Model Species of UO_2(bdc)(dmpi) and the Free Uranyl Cation

species	s	p	d	f
UO_2(bdc)(dmpi)	4.139	12.054	11.745	2.512
UO_2^{2+}	4.030	11.797	11.450	2.646

It should be noted that the small-core RECPs attribute $5s^25p^65d^{10}6s^26p^6$ as the ground-state valence subconfigurations for U(VI). According to our calculations (Table 3), Mulliken orbital populations show relatively higher charge populations in the valence 6d shells for uranium in UO_2(bdc)(dmpi) compared to the free uranyl cation, and this change is rooted in the impact of electronegative imidazole. Moreover, the uranium 5f shell is slightly less occupied in UO_2(bdc)(dmpi) than that in UO_2^{2+}. These results suggest that the bending of uranyl in UO_2(bdc)(dmpi) attributed to a greater 6d orbital and less occupied 5f shell of uranium.

Fluorescence Spectra and Powder X-ray Diffraction. Most of the uranyl compounds containing the UO_2^{2+} moiety can emit green light from 450 to 600 nm with strong vibrational coupling, yielding a well-resolved five-peak pattern. The

DOI: 10.1021/acs.inorgchem.5b00013
Inorg. Chem. 2015, 54, 3829−3834

fluorescence spectra of UO_2(bdc)(dmpi) were measured on a Hitachi F-4600 fluorescence spectrophotometer. As illustrated in Figure S2, Supporting Information, UO_2(bdc)(dmpi) can emit green light when excited at 310 nm, and the emission peaks are resolved at 526, 546, 567, 589, and 617 nm. These emission peaks are attributed to the transitions from the first excited electronic level to the symmetric and antisymmetric vibration levels of the uranyl ion. Compared with uranyl nitrate whose emission peaks are located at 488, 510, 534, 560, and 588 nm, UO_2(bdc)(dmpi) reveals a remarkable red-shifted fluorescence spectra. The remarkable red shift of 38 nm is greater than those of the compounds reported in the literature,[41,42] in which the compounds have a red shift of 10 and 27 nm, respectively, compared with uranyl nitrate as well. The red shift may be caused by various influencing factors such as disorder within the equatorial plane of the uranyl group or a distinct coordination pattern around the UO_2^{2+} moiety, etc.[41] In addition, the PXRD data of UO_2(bdc)(dmpi) is shown in Figure S1, Supporting Information, which coincides well with the simulated pattern. This proves the synthesized material is identical with the measured single crystals.

CONCLUSION

In this work, a new uranyl organic framework, UO_2(bdc)(dmpi), was hydrothermally synthesized using H_2bdc and dmpi. It exhibits a new 3-fold interpenetrated (2,4)-connected topology with the Schläfli symbol of $(12^6)(12)_2$. Large incurvation of UO_2^{2+} was found for the first time in a 3-fold interpenetrated framework. In addition, theoretical calculations found that in UO_2(bdc)(dmpi) the uranium 6d shells showed higher occupations than the free uranyl cation, and the uranium 5f shell was less occupied in UO_2(bdc)(dmpi) than that in UO_2^{2+}, implying the change in the uranium 5f/6d orbital made a greater contribution to the bent uranyl in UO_2(bdc)(dmpi), and imidazoles close to uranyl played a significant role in this change. Guided under the experimental and theoretical studies, it can be predicted that a larger incurvation in uranyl compounds would be found if uranyl interacted with a more electronegative heterocyclic compound, and this incurvation could provide new insight into the reactivity and functionalization of uranyl ions.

ASSOCIATED CONTENT

Supporting Information

Crystallographic data for UO_2(bdc)(dmpi) in CIF format; solid-state fluorescence spectra and PXRD pattern of UO_2(bdc)(dmpi); information about selected bond lengths and angles. This material is available free of charge via the Internet at http://pubs.acs.org.

AUTHOR INFORMATION

Corresponding Author

*E-mail: zfchai@suda.edu.cn.

Author Contributions

Fei Chen and Cong-zhi Wang contributed equally.

Notes

The authors declare no competing financial interest.

ACKNOWLEDGMENTS

This work was supported by the National Natural Science Foundation of China (Grant Nos. 21101157, 21201166, and 11205169).

REFERENCES

(1) Nouar, F.; Eckert, J.; Eubank, J. F.; Forster, P.; Eddaoudi, M. *J. Am. Chem. Soc.* **2009**, *131*, 2864−2870.
(2) Li, K.; Olson, D. H.; Lee, J. Y.; Bi, W.; Wu, K.; Yuen, T.; Xu, Q. L. *J. Adv. Funct. Mater.* **2008**, *18*, 2205−2214.
(3) Ayyappan, P.; Evans, O. R.; Cui, Y.; Wheeler, K. A.; Lin, W. *Inorg. Chem.* **2002**, *41*, 4978−4980.
(4) Devic, T.; Salles, F.; Bourrelly, S.; Moulin, B.; Maurin, G.; Horcajada, P.; Serre, C.; Vimont, A.; Lavalley, J. C.; Leclerc, H.; Clet, G.; Daturi, M.; Llewellyn, P. L.; Filinchuk, Y.; Férry, G. *J. Mater. Chem.* **2012**, *22*, 10266−10273.
(5) Haldoupis, E.; Nair, S.; Sholl, D. S. *J. Am. Chem. Soc.* **2012**, *134*, 4313−4323.
(6) Xu, H.; Liu, F.; Cui, Y.; Chen, B.; Qian, G. *Chem. Commun.* **2011**, *47*, 3153−3155.
(7) Luz, I.; Xamena, F. X. L.; Corma, A. *J. Catal.* **2012**, *285*, 285−291.
(8) Pan, L.; Adams, K. M.; Hernandez, H. E.; Wang, X.; Zheng, C.; Hattori, Y.; Kaneko, K. *J. Am. Chem. Soc.* **2003**, *125*, 3062−3067.
(9) Eddaoudi, M.; Kim, J.; Rosi, N.; Vodak, D.; Wachter, J.; O'Keeffe, M.; Yaghi Omar, M. *Science* **2002**, *295*, 469−472.
(10) Burns, P. C. *Mineral. Mag.* **2011**, *75*, 1−25.
(11) Schindler, M.; Mutter, A.; Hawthorne, F. C.; Putnis, A. *Can. Mineral.* **2004**, *42*, 1651−1666.
(12) Unruh, D. K.; Baranay, M.; Pressprich, L.; Stoffer, M.; Burns, P. C. *J. Solid State Chem.* **2012**, *186*, 158−164.
(13) Brugger, J.; Krivovichev, S. V.; Berlepsch, P.; Meisser, N.; Ansermet, S.; Armbruster, T. *Am. Mineral.* **2004**, *89*, 339−347.
(14) Chen, C. S.; Kao, H. M.; Lii, K. H. *Inorg. Chem.* **2005**, *44*, 935−940.
(15) Thuéry, P.; Masci, B. *CrystEngComm* **2012**, *14*, 131−137.
(16) Wu, H. Y.; Wang, R. X.; Yang, W.; Chen, J.; Sun, Z. M.; Jun, L.; Zhang, H. *Inorg. Chem.* **2012**, *51*, 3103−3107.
(17) Arnold, P. L.; Jones, G. M.; Odoh, S. O.; Schreckenbach, G.; Magnani, N.; Love, J. B. *Nat. Chem.* **2012**, *4*, 221−227.
(18) Otwinowski, Z.; Minor, W. *Macromolecular Crystallography, Part A*; Academic Press: New York, 1997.
(19) Sheldrick, G. M. *SHELXL-97: Program for Crystal Structure Refinement*; University of Göttingen: Germany, 1997.
(20) Frisch, M. J.; Trucks, G. W.; Schlegel, H. B.; Scuseria, G. E.; Robb, M. A.; Cheeseman, J. R.; Montgomery, Jr., J. A.; Vreven, T.; Kudin, K. N.; Burant, J. C.; Millam, J. M.; Iyengar, S. S.; Tomasi, J.; Barone, V.; Mennucci, B.; Cossi, M.; Scalmani, G.; Rega, N.; Petersson, G. A.; Nakatsuji, H.; Hada, M.; Ehara, M.; Toyota, K.; Fukuda, R.; Hasegawa, J.; Ishida, M.; Nakajima, T.; Honda, Y.; Kitao, O.; Nakai, H.; Klene, M.; Li, X.; Knox, J. E.; Hratchian, H. P.; Cross, J. B.; Bakken, V.; Adamo, C.; Jaramillo, J.; Gomperts, R.; Stratmann, R. E.; Yazyev, O.; Austin, A. J.; Cammi, R.; Pomelli, C.; Ochterski, J. W.; Ayala, P. Y.; Morokuma, K.; Voth, G. A.; Salvador, P.; Dannenberg, J. J.; Zakrzewski, V. G.; Dapprich, S.; Daniels, A. D.; Strain, M. C.; Farkas, O.; Malick, D. K.; Rabuck, A. D.; Raghavachari, K.; Foresman, J. B.; Ortiz, J. V.; Cui, Q.; Baboul, A. G.; Clifford, S.; Cioslowski, J.; Stefanov, B. B.; Liu, G.; Liashenko, A.; Piskorz, P.; Komaromi, I.; Martin, R. L.; Fox, D. J.; Keith, T.; Al-Laham, M. A.; Peng, C. Y.; Nanayakkara, A.; Challacombe, M.; Gill, P. M. W.; Johnson, B.; Chen, W.; Wong, M. W.; Gonzalez, C.; Pople, J. A. *Gaussian 09*, Revision A.02; Gaussian, Inc.: Wallingford, CT, 2009.
(21) Becke, A. D. *J. Chem. Phys.* **1993**, *98*, 5648−5652.
(22) Lee, C.; Yang, W.; Parr, R. G. *Phys. Rev. B* **1988**, *37*, 785−789.
(23) Kuchle, W.; Dolg, M.; Stoll, H.; Preuss, H. *J. Chem. Phys.* **1994**, *100*, 7535−7542.
(24) Cao, X.; Dolg, M. *J. Mol. Struct. (THEOCHEM)* **2004**, *673*, 203−209.
(25) Dolg, M.; Stoll, H.; Preuss, H. *J. Chem. Phys.* **1989**, *90*, 1730−1734.
(26) Vetere, V.; Maldivi, P.; Adamo, C. *J. Comput. Chem.* **2003**, *24*, 850−858.
(27) Santo, E. Di; Santos, M.; Michelini, M. C.; Marcalo, J.; Russo, N.; Gibson, J. K. *J. Am. Chem. Soc.* **2011**, *133*, 1955−1970.

DOI: 10.1021/acs.inorgchem.5b00013
Inorg. Chem. 2015, 54, 3829−3834

(28) Michelini, M. C.; Russo, N.; Sicilia, E. *J. Am. Chem. Soc.* **2007**, *129*, 4229−4239.
(29) Reed, A. E.; Curtiss, L. A.; Weinhold, F. *Chem. Rev.* **1988**, *88*, 899−926.
(30) Reed, A. E.; Weinstock, R. B.; Weinhold, F. *J. Chem. Phys.* **1985**, *83*, 735−746.
(31) Kovacs, A.; Konings, R. J. M. *J. Phys. Chem. Ref. Data* **2004**, *33*, 377−404.
(32) Pantazis, D. A.; Neese, F. *J. Chem. Theory Comput.* **2009**, *5*, 2229−2238.
(33) Shannon, R. D. *Acta Crystallogr.* **1976**, *A32*, 751−767.
(34) Spek, A. L. *Platon: A Multi-purpose Crystallographic Tool*; Utrecht University: Utrecht, The Netherlands, 2001.
(35) Lu, T.; Chen, F. *J. Comput. Chem.* **2012**, *33*, 580−592.
(36) Becke, A. D.; Edgecombe, K. E. *J. Chem. Phys.* **1990**, *92*, 5397−5403.
(37) Tatsumi, K.; Hoffmann, R. *Inorg. Chem.* **1980**, *19*, 2656−2658.
(38) Wadt, W. R. *J. Am. Chem. Soc.* **1981**, *103*, 6053−6057.
(39) Pyykko, P.; Laakkonen, L. J.; Tatsumi, K. *Inorg. Chem.* **1989**, *28*, 1801−1805.
(40) Dyall, K. G. *Mol. Phys.* **1999**, *96*, 511−518.
(41) Chen, F.; Wang, C.; Shi, W.; Zhang, M.; Liu, C.; Zhao, Y.; Chai, Z. *CrystEngComm* **2013**, *15*, 8041−8048.
(42) Tian, T.; Yang, W.; Pan, Q.; Sun, Z. *Inorg. Chem.* **2012**, *51*, 11150−11154.

DOI: 10.1021/acs.inorgchem.5b00013
Inorg. Chem. 2015, 54, 3829−3834